Acta Crystallographica Section B
Structural Science
ISSN 0108-7681

Electron density study of 2*H*-chromene-2-thione

Parthapratim Munshi and T. N. Guru Row*

Solid State and Structural Chemistry Unit, Indian Institute of Science, Bangalore – 560012, India

Correspondence e-mail: ssctng@sscu.iisc.ernet.in

Received 7 June 2002
Accepted 11 October 2002

The charge-density distribution in 2*H*-chromene-2-thione (2-thiocoumarin), C_9H_6OS, has been determined from X-ray diffraction data measured at 90 K using a CCD detector, to a resolution of $\sin\theta/\lambda < 1.08$ Å^{-1}. A multipolar-atom density model was fitted against 6908 reflections with $I > 2\sigma(I)$ [$R(F) = 0.021$, $wR(F) = 0.022$, goodness of fit = 1.81] in order to generate the difference Fourier maps. The topological properties of the molecular electron density in terms of the bond critical points and the evaluation of the dipole moment show that the molecular dipole moment in the crystal is higher than the corresponding value derived from theoretical calculations.

1. Introduction

Experimental charge densities can be used to analyze a range of problems of chemical interest (Coppens, 1997) since the charge density is a physically observable quantity. An accurate experimental measurement and analysis of charge density in a molecular crystal can be obtained using high-resolution X-ray diffraction data at low temperatures (Coppens, 1998). Recent technological developments in area detectors provide faster means of obtaining such high-quality data sets (Martin & Pinkerton, 1998; Dahaoui *et al.*, 1999; Volkov *et al.*, 1999). Generally data sets are collected using conventional generators equipped with high-sensitivity two-dimensional CCD detectors at temperatures of about 100 K. Such data sets provide redundant data of high quality on molecular crystals (Coppens *et al.*, 1999; Ellena *et al.*, 2001; Slouf *et al.*, 2002). One of the most exciting applications of charge-density analysis is the evaluation of one-electron properties in molecular crystals. The widely used approach for this purpose is the Hansen–Coppens formalism (Hansen & Coppens, 1978), in which the individual atomic densities are described in terms of a spherical core and valence densities together with an expansion of the atom-centered spherical-harmonic functions. Also, the topology of the charge density is manifested as local maxima at the positions of the nuclei, as can be inferred from Bader's quantum theory (Bader, 1990). The maxima of the electron density are then the *critical points* at which the first derivatives of the density become zero. The second derivative of the density, the *Laplacian*, represents the chemical features of the molecule.

Coumarin is a simple organic molecule that has featured in several areas of synthetic chemistry, medicinal chemistry and photochemistry (Vishnumurthy *et al.*, 2001). Several substituted coumarin derivatives are used in the dye industry (Hooper *et al.*, 1982; Morris & Russell, 1971). These coumarins have also been studied extensively as laser dyes (Khalfan *et al.*,

1987) and have shown state-dependent variation in the static dipole moment. Coumarins have been employed as probes for the examination of ultrafast solvation effects (Maroncelli & Fleming, 1987). Theoretical calculations using semi-empirical methods demonstrate that coumarin and its sulfur derivatives possess well defined dipole moments. In addition, the sulfur derivatives of coumarin crystallize in non-centrosymmetric space groups (Munshi & Guru Row, 2001, 2002). These features are responsible for coumarin and its derivatives to exhibit second-harmonic generation (SHG) effects. We have studied the geometry and the molecular-packing patterns of several coumarins and its derivatives (Vishnumurthy *et al.*, 2001) in order to evaluate the features of non-covalent interactions. In an effort to generate materials that possess a larger dipole moment than coumarin, we have recently synthesized and studied the structures of the sulfur derivatives (Munshi & Guru Row, 2001, 2002). An accurate high-resolution charge-density study followed by a topological analysis will provide insights into the factors responsible for the large static dipole moment. The value of the dipole moment can be determined from the multipole model fitted to the experimental X-ray diffraction data. The value thus obtained can be compared with the theoretical value determined either based on the density functional theory (DFT) or the Hartree–Fock (HF) approach using the *GAUSSIAN*98 package (Frisch *et al.*, 2002).

Charge-density studies involving S atoms are rare in the literature. To our knowledge, the charge-density distribution has been analyzed for only five molecules that contain sulfur (Bats & Coppens, 1977; Weber & Craven, 1987; Fabius *et al.*, 1989; Scherer *et al.*, 2000), and the nature of the multipolar expansion around sulfur is not fully understood. This study will be the first example of a C═S case, and the evaluation of the charge-density parameters will be of interest. This paper presents the charge-density distribution and the topological properties of 2*H*-chromene-2-thione (2-thiocoumarin).

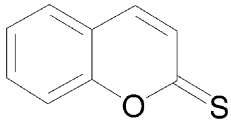

2. Experimental

The crystal structure of 2-thiocoumarin has been reported earlier at room temperature (Munshi & Guru Row, 2001). Preliminary theoretical estimates of the dipole moment, which were made using *GAUSSIAN*98 and which were based on the coordinates obtained from the above experiment, suggested that the molecular dipole moment is about 6.5 Debye.

A slow-evaporation method at low temperature was used to recrystallize the compound from chloroform and hexane (1:4), in order to generate crystals of better quality for the charge-density study. A good-quality crystal (0.60 × 0.37 × 0.10 mm) was selected for the X-ray diffraction study and was mounted in a Lindemann capillary at room temperature. The sample was cooled to 90 K (ramp rate 120 K h^{-1}) with an Oxford Cryostream N_2 open-flow cryostat. The crystal was allowed to stabilize at 90 K for 1 h, and the unit-cell parameters were determined every 15 min thereafter until the estimated standard deviations in cell dimensions did not vary beyond acceptable limits. Three batches of data were collected as follows: the first covered the whole sphere of reciprocal space up to ∼55° in 2θ; the second higher-order batch covered up to ∼77° in 2θ; and the final high order covered up to ∼100° in 2θ. For each data set, 2424 frames were collected with a scan width of 0.3° in ω and an exposure time of 15 s, 30 s and 45 s per frame, respectively. The details of the data-collection strategy are summarized in Table 1. The entire data set, which consisted of 7272 frames, was collected over a period of ∼80 h and was monitored with the *SMART* software package (Bruker, 1998). The frames were then integrated with *SAINT* (Bruker, 1998) using a narrow-frame integration method. A total of 9651 reflections were used for the determination of the unit-cell parameters. Of the 37982 reflections obtained from *SAINT*, 37879 were accepted for sorting, averaging and scaling by the program *SORTAV* (Blessing, 1987). Of the 37879 integrated reflections, 2053 were rejected as outliers and 35826 were accepted. 642 reflections were measured only once, 1543 were measured twice and 5423 were measured three or more times. After merging the data, a total of 7608 unique reflections to a resolution of $\sin\theta/\lambda < 1.08$ Å^{-1} ($D_{\min} = 0.46$ Å) were recovered with an overall completeness of 99.2%. All 35826 intensities were corrected for decay, beam inhomogeneity and absorption effects ($T_{\min} = 0.808$, $T_{\max} = 0.964$). The internal agreement factor for the final data set is $R_{\rm int} = 0.038$. No problems from the $\lambda/2$ contamination appeared in the entire data set.

Table 1
A summary of the 90 K X-ray data collection strategy.

Run	Frame	2θ (°)	ω (°)	φ (°)	χ (°)	Axis	Width (°)	No. of frames	Time (s)
1	001	−25	−25	0	54.79	2	0.3	606	15
2	001	−25	−25	90	54.79	2	0.3	606	15
3	001	−25	−25	180	54.79	2	0.3	606	15
4	001	−25	−25	270	54.79	2	0.3	606	15
5	001	−50	−50	0	54.79	2	0.3	606	30
6	001	−50	−50	90	54.79	2	0.3	606	30
7	001	−50	−50	180	54.79	2	0.3	606	30
8	001	−50	−50	270	54.79	2	0.3	606	30
9	001	−75	−75	0	54.79	2	0.3	606	45
10	001	−75	−75	90	54.79	2	0.3	606	45
11	001	−75	−75	180	54.79	2	0.3	606	45
12	001	−75	−75	270	54.79	2	0.3	606	45

3. Structure refinement

The structure was solved by direct methods using *SHELXS*97 and refined in the spherical-atom approximation using *SHELXL*97 (Sheldrick, 1997). Fig. 1 gives the *ORTEP* (Farrugia, 1997) diagram together with the numbering of the atoms. All H atoms were located by the difference-Fourier method and were refined isotropically; other non-H atoms

were refined anisotropically. The refinements were based on F^2 and were performed using all 7608 reflections, which converged at $R(F) = 0.033$, $wR(F) = 0.088$ and goodness of fit = 1.036. Fig. 2 shows the packing of the molecules in the crystal lattice viewed along the *b* axis. The molecules pack in an antiparallel fashion that generates an overall herringbone-like structure, and the interactions are stabilized mainly by van der Waals interactions. The aspherical-atom refinement was based on *F* and was carried out, using the *XD* package (Koritsanszky *et al.*, 1999), on 6908 reflections with $I > 2\sigma(I)$. The *XD* package consists of a least-squares refinement program based on the Hansen–Coppens multipole formalism (Hansen & Coppens, 1978). Initially only the scale factor was refined on all data, in order to check the accuracy of the data transfer from *SHELX* to *XD via XDINI*. The real and imaginary dispersion corrections to the form factors (*International Tables for Crystallography*, 1992, Vol. C, pp. 206–222) were used in all the structure-factor calculations. Next, the higher-order refinement was performed using 3838 reflections with $0.8 < \sin\theta/\lambda < 1.08$ Å^{-1} and $I > 2\sigma(I)$. This refinement resulted in accurate positional coordinates and thermal parameters for all non-H atoms. The values of the maximum differences of the mean square displacement amplitudes (DMSDA) (Hirshfeld, 1976) indicate the inadequacies in the model at convergence. These values should be less than 0.001 Å^2 for bonds between carbon-like atoms for correct models. In the current experiment the value of DMSDA at the convergence of the refinement [$R(F) = 0.029$, $wR(F) = 0.032$, where $w = 1/\sigma^2(F^2)$ and goodness of fit = 1.22] has a maximum value for the C1—S1 bond ($\Delta Z^2 = 6 \times 10^{-4}$ Å^2) suggesting that the model is adequate. The positional and isotropic thermal parameters of the H atoms were then refined using the lower-angle data ($0.057 < \sin\theta/\lambda < 0.8$ Å^{-1}). Further multipolar refinement was carried out in the following manner using all 6908 reflections with $I > 2\sigma(I)$. Initially the scale factor and monopole populations for all atoms were refined, and then a single κ refinement was performed. However, the positions of the H atoms in this refinement, as well as in the subsequent refinements, were fixed using the reset bond option, which constrains the H atoms to average bond-distance values that are determined from neutron-diffraction studies (Allen, 1986). Refinements that released dipole, quadrupole, octapole and hexadecapole (hexadecapole only for S and O atoms) populations with a single κ value were performed in a stepwise manner. At each step the refinements were cycled until convergence. Finally a single κ' was refined for each species for all non-H atoms along with the rest of the parameters. No extinction correction was applied during the refinements. Tests on isotropic *type*1 and *type*2 corrections did not significantly change the quality of the residual maps. The maximum DMSDA value is $\Delta Z^2 = 5 \times 10^{-4}$ Å^2 for the C8—C7 bond. The good quality of the final model is also indicated by Fig. 3, which maps the residual density in the molecular plane as obtained in the final cycle of the refinement. Table 2 lists relevant experimental details.

4. Results and discussion

Atomic coordinates, equivalent isotropic displacement parameters, anisotropic thermal parameters, bond lengths, angles,

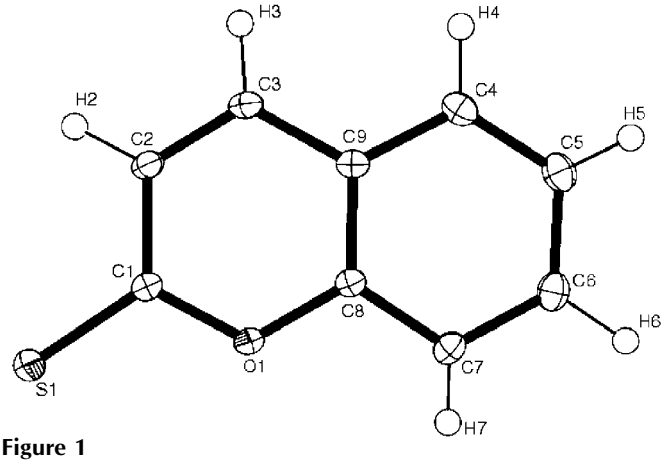

Figure 1
ORTEP diagram of the molecule showing the numbering scheme used in this work. Thermal ellipsoids are drawn at the 50% probability level.

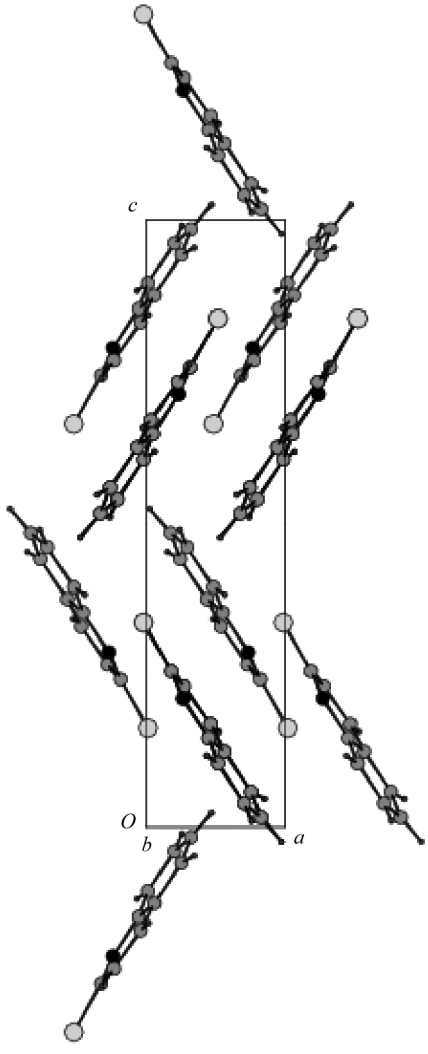

Figure 2
Molecular packing of the crystal viewed along the *b* axis.

Table 2
Experimental details.

Crystal data	
Chemical formula	C_9H_6OS
Chemical formula weight	162.21
Cell setting, space group	Orthorhombic, $P2_12_12_1$
a, b, c (Å)	4.0515 (2), 10.1749 (7), 17.6519 (9)
V (Å^3)	727.67 (7)
Z	4
D_x (Mg m^{-3})	1.481
Radiation type	Mo $K\alpha$
No. of reflections for cell parameters	9651
θ range (°)	2.31–50.08
μ (mm^{-1})	0.369
Temperature (K)	90.0 (2)
Crystal form, color	Prism, yellow
Crystal size (mm)	0.60 × 0.37 × 0.10
Data collection	
Diffractometer	CCD area detector Bruker AXS SMART APEX
Data collection method	φ and ω scans
Absorption correction	Empirical
T_{min}	0.8088
T_{max}	0.9640
No. of measured, independent and observed reflections	37982, 7608, 6908
Criterion for observed reflections	$I > 2\sigma(I)$
R_{int}	0.038
θ_{max} (°)	50.11
Range of h, k, l	$0 \rightarrow h \rightarrow 8$ $0 \rightarrow k \rightarrow 21$ $-37 \rightarrow l \rightarrow 37$
Extinction correction	None
Refinement	
Refinement on	F
R, wR, S	0.0217, 0.0223, 1.8112
No. of reflections and parameters used in refinement	6908, 318
H-atom treatment	No refinement
Weighting scheme	$w = 1/[\sigma^2(F_o^2)]$
$(\Delta/\sigma)_{max}$	0.002
$\Delta\rho_{max}$, $\Delta\rho_{min}$ (e Å^{-3})	0.199, −0.276
Flack parameter	−0.01 (3)

Computer programs used: Bruker *SMART*, Bruker *SAINT* (Bruker, 1998), *SHELXS*97 (Sheldrick, 1997), *XD* (Koritsanszky *et al.*, 1999).

dihedral angles and the charge density parameters P_v and $P_{lm\pm}$ have been deposited as supplementary material.[1] The molecules in the crystal lattice are held together only *via* van der Waals interactions.

The residual density map (Fig. 3) is reasonably clear of noise, and therefore the high quality of the data is confirmed. It can be seen that there is an accumulation of residual charge density in the vicinity of the S atom, which could be due to the possible nature of polarization and also due to the deficiencies in the multipole model to account for the overall density at this site. The experimental dynamic-deformation density map, which is given in Fig. 4(*a*), is calculated using 3955 reflections per octant with $\sin\theta/\lambda < 1.08$ Å^{-1} and $I > 2\sigma(I)$. The corresponding static-deformation density map, which is calculated based on the difference between the atom-centered multipole

[1] Supplementary data for this paper are available from the IUCr electronic archives (Reference: LC0053). Services for accessing these data are described at the back of the journal.

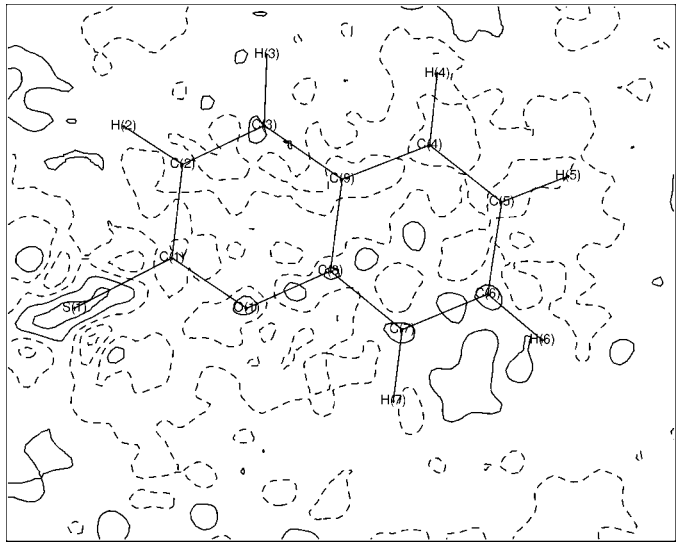

Figure 3
Residual density map in the molecular plane. The first positive contour is at 0.05 e Å^{-3} and the contour levels are at 0.1 e Å^{-3} intervals. The negative contours start at −0.05 e Å^{-3} and the contour levels are at −0.1 e Å^{-3} intervals. The solid lines are positive contours and the broken lines are negative contours.

density and the charge distribution of the pro-molecule density, is given in Fig. 4(*b*). The lone pairs on the S and the O atoms are clearly visible in both these maps.

In an effort to make a quantitative analysis of these observations, the nature of the bonding features was investigated. For every chemical bond in the structure there is a point at which the first derivative of the charge density vanishes (Bader, 1990). There are three non-zero principle curvatures – two with negative values and one with a positive value – in the bonding density, ρ_b, at this bond critical point (BCP). Such a BCP is labeled (3, −1): 3 for the number of non-zero curvatures and −1 for the algebraic sum of the curvature signs. The (3, −1) BCPs of the charge density were evaluated, and Fig. 5 shows the BCPs in the molecule along with the paths that link the atoms, which are referred to as the bond paths. Table 3 lists the bonding between atoms; the value of the charge density, $\rho_b(\mathbf{r})$; the Laplacian, $\nabla^2\rho_b(\mathbf{r})$; $D1$ and $D2$, the distances to the BCP from the first and second atom, respectively; the eigenvalues of the Hessian matrix; and the bond ellipticity, ε. The values of these quantities in our analysis of the aromatic portion of the structure are similar to those generally found in aromatic moieties (Ellena *et al.*, 2001). The double-bond nature of the C═S bond is clearly indicated by its ε value (0.26) and by the nearly equal values of $D1$ and $D2$ for this bond. The critical points on the C1—O1 and C8—O1 bonds are shifted from the bond midpoints; their ε values are 0.11 and 0.12, respectively, which suggest a high degree of polarization in these bonds. The value of $\nabla^2\rho_b(\mathbf{r})$ on the C═S bond is significantly large (−3.264), and the corresponding bonding density, ρ_b, is significantly low (1.558). These values indicate that the charge density is drawn out into the lone-pair region of the S atom. These features will certainly influence the one-

electron properties and hence will have a bearing on the calculated dipole moment components. Fig. 6 shows the experimental Laplacian $\nabla^2\rho_b(\mathbf{r})$, which clearly shows the features of all the intramolecular interactions. At the end of the refinement the P_v value of the S atom is 5.29 (4) while that of the O atom is 6.28 (4), and these values depict the nature of the charge distribution in the valence shell in this molecule. The refined κ-parameters show a contraction of the S atom ($\kappa = 1.16$) while the O atom remains intact ($\kappa = 1.00$). However, all C atoms show a slight contraction ($\kappa = 1.03$). The corresponding κ' values are 0.85 for S, 0.96 for O and 0.88 for C atoms.

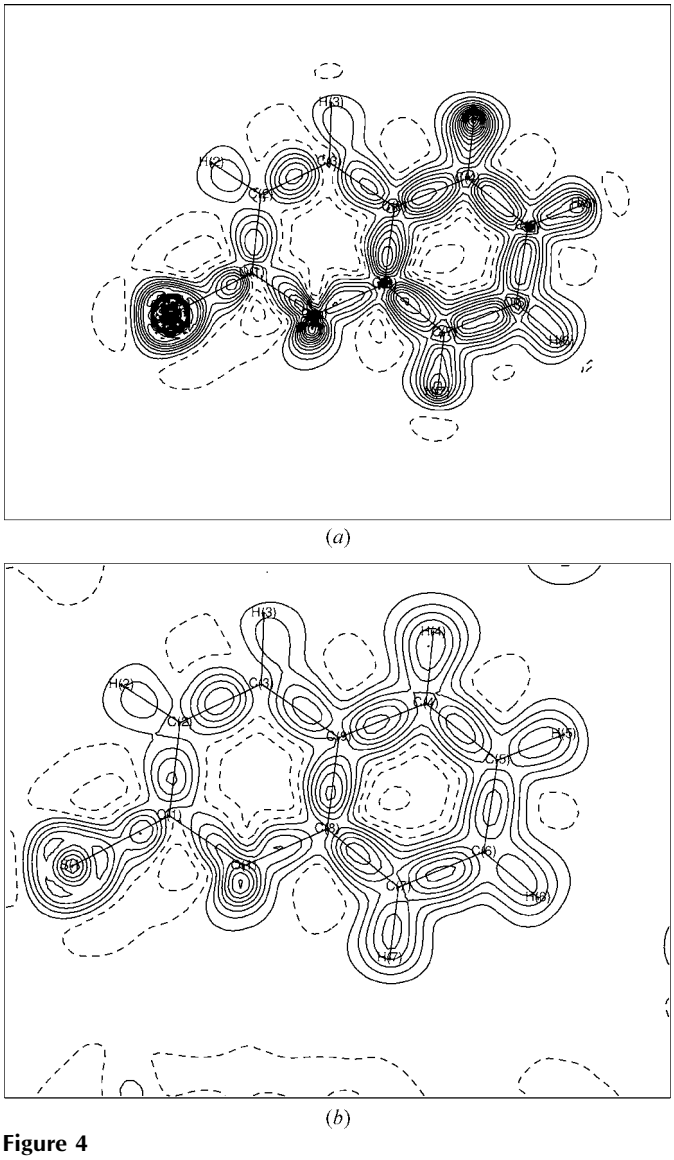

Figure 4
(*a*) Dynamic-deformation density map in the plane of the molecule. The first positive contour is at 0.05 e Å^{-3} and the contour levels are at 0.1 e Å^{-3} intervals. The first negative contour is at −0.05 e Å^{-3} and the contour levels are at −0.1 e Å^{-3} intervals. The solid lines are positive contours and the broken lines are negative contours. (*b*) Static-deformation density map in the plane of the molecule. The positive contour levels are at 0.1 e Å^{-3} intervals and the negative contour levels are at −0.1 e Å^{-3} intervals. The solid lines are positive contours and the broken lines are negative contours.

Table 3
Intramolecular bond critical points and their properties.

Bond	$\rho_b(\mathbf{r})$	$\nabla^2\rho_b(\mathbf{r})$	$D1$	$D2$	λ_1	λ_2	λ_3	ε
S(1)−C(1)	1.558	−3.264	0.8215	0.8340	−10.16	−8.06	14.95	0.26
O(1)−C(8)	2.112	−19.235	0.8193	0.5574	−18.58	−16.55	15.90	0.12
O(1)−C(1)	1.995	−18.421	0.8504	0.5137	−17.13	−15.43	14.13	0.11
C(8)−C(9)	2.150	−20.449	0.7335	0.6652	−17.82	−13.63	11.00	0.31
C(8)−C(7)	2.198	−20.085	0.7336	0.6615	−17.41	−13.99	11.32	0.24
C(3)−C(9)	2.020	−15.567	0.7060	0.7288	−15.31	−12.70	12.45	0.21
C(3)−C(2)	2.490	−25.702	0.7191	0.6402	−20.28	−16.36	10.94	0.24
C(9)−C(4)	2.213	−19.265	0.7231	0.6882	−17.14	−14.14	12.02	0.21
C(2)−C(1)	1.954	−15.685	0.6852	0.7507	−14.86	−12.37	11.54	0.20
C(4)−C(5)	2.150	−19.134	0.7019	0.6844	−17.07	−13.63	11.57	0.25
C(7)−C(6)	2.324	−17.907	0.6862	0.7056	−17.36	−13.83	13.29	0.26
C(6)−C(5)	2.073	−15.821	0.7031	0.7024	−15.59	−12.78	12.55	0.22

Since our main aim is to obtain an accurate molecular dipole moment, the program *XDPROP* from the *XD* package is employed to obtain the components of the dipole moment. Table 4 gives the values of the components and the value of the net dipole moment that are obtained from the experiment. Table 4 also provides the values for the dipole moments as obtained from theoretical calculations based on the package *GAUSSIAN*98. The calculations have been performed using both HF and DFT methods. The DFT method (basis set 6-311G**) produces a dipole moment that is significantly smaller than that obtained using the *ab initio* HF method at the same level. The molecular geometry as found in the final refinement has been adopted in all the calculations. In the charge-density analysis of a polar molecule, 2-methyl-4-nitroaniline (Howard *et al.*, 1992), it is observed that the experimentally determined value of the dipole moment is rather high compared with the theoretically determined value. A similar feature is also observed in the structure of 2-thiocoumarin. The main contributors to the dipole-moment components are the S and the O atoms in this structure. The coordinates and the population parameters of the valence shell P_v, and their corresponding values of P_{11+}, P_{10}, P_{11-} and

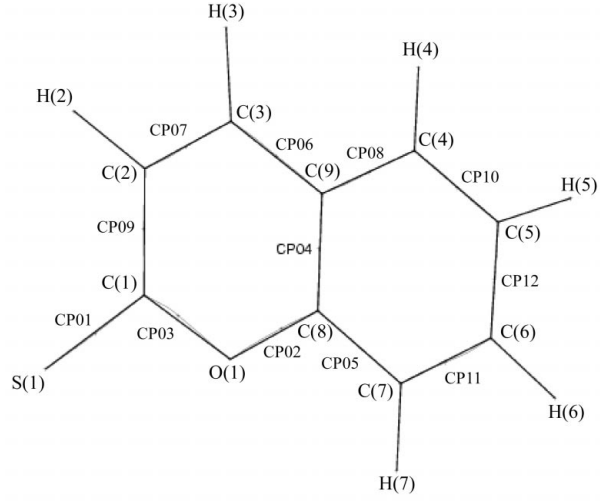

Figure 5
Bond-path character in the molecule showing the critical-point locations along the bonds.

Table 4
Molecular dipole moment of 2-thiocoumarin†.

	μ_x	μ_y	μ_z	$\lvert\mu\rvert$
X-ray diffraction	15.2	1.1	0.4	15.2
HF/6-21G**	5.9	2.4	0.0	6.4
HF/6-31G**	6.0	2.6	0.0	6.6
HF/6-311G**	5.9	2.6	0.0	6.5
B3LYP/6-311G**	5.2	2.3	0.0	5.7

† All values in Debyes.

κ, form the basis of the evaluation of the dipole moment. Since, in the compound under study, the influence of the polarization of the charge density is dominant at these atomic sites, the resulting dipole-moment values differ substantially from theoretical values. It must be noted that the coordinates in both theory and experimental calculations refer to the same orientation of the molecule. As discussed earlier the values of ε and $D1$ and $D2$ in the bonds associated with the O atom and the rather large value of $\nabla^2\rho_b(\mathbf{r})$ in the C═S region appear to contribute to the large value of the dipole moment (15.2 Debye). Recently, a careful evaluation of molecular dipole moments from the multipole refinement of X-ray diffraction data (Abramov *et al.*, 1999; Arnold *et al.*, 2000) has shown the influence of the crystal lattice on the enhancement of molecular dipole moments. The limitations in theory (Bader, 1990) to define the topology of the molecular boundary could also influence the differences seen in theory and experiment. Experimental charge-density analyses of yet another sulfur-containing coumarin, 2*H*-thiochromen-2-one, and of coumarin itself are currently being investigated by us in order to obtain better insights into the dipole-moment behavior in this class of compounds.

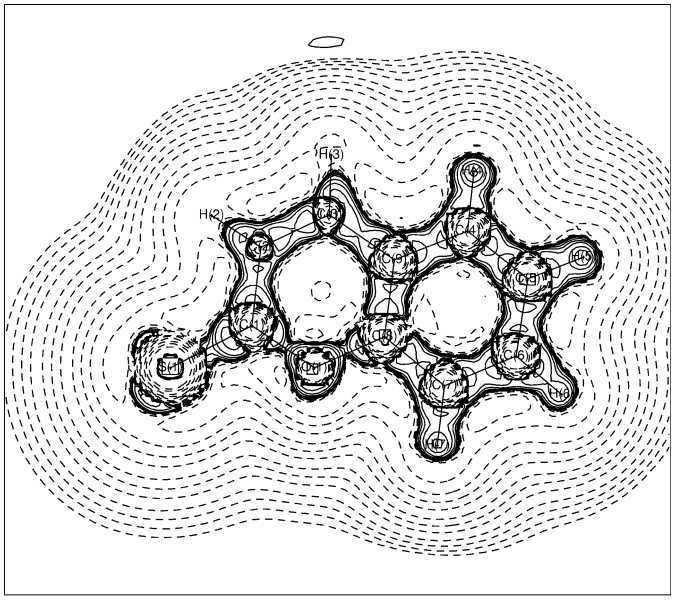

Figure 6
Laplacian $[\nabla^2\rho_b(\mathbf{r})]$ distribution in the plane of the molecule. Contours are drawn at logarithmic intervals in $-\nabla^2\rho_b$ e Å^{-5}. The solid lines are positive contours and the broken lines are negative contours.

5. Conclusion

The multipolar model based on the electron density of 2-thiocoumarin confirms the presence of a large molecular dipole moment and suggests the possibility of generating a new series of SHG materials. Topological analysis reveals the nature of the charge distribution and bonding features in this molecule. The experimental values for the dipole moment are high compared with the theoretical values, which suggests possible inadequacies in the multipolar expansion for highly polarized molecular crystals.

We thank the Department of Science and Technology, India for data collection on the CCD facility setup under the IRFA-DST program.

References

Abramov, Y., Volkov, A. & Coppens, P. (1999). *Chem. Phys. Lett.* **311**, 81–86.
Allen, F. H. (1986). *Acta Cryst.* B**42**, 515–522.
Arnold, W. D., Sanders, L. K., McMahon, M. T., Volkov, A. V., Wu, G., Coppens, P., Wilson, S. R., Godbout, N. & Oldfield, E. (2000). *J. Am. Chem. Soc.* **122**, 4708–4717.
Bader, R. F. W. (1990). *Atoms in Molecules – A Quantum Theory*. Oxford: Clarendon.
Bats, J. W. & Coppens, P. (1977). *Acta Cryst.* B**33**, 37–45; 1542–1548.
Blessing, R. H. (1987). *Crystallogr. Rev.* **1**, 3–58.
Bruker (1998). *SMART. SAINT.* Bruker AXS Inc., Madison, Wisconsin, USA.
Coppens, P. (1997). *X-ray Charge Densities and Chemical Bonding*. New York: Oxford University Press.
Coppens, P. (1998). *Acta Cryst.* A**54**, 779–788.
Coppens, P., Abramov, Y., Carducci, M., Korjov, B., Novozhilova, I., Alhmbra, C. & Pressprich, M. R. (1999). *J. Am. Chem. Soc.* **121**, 2585–2593.
Dahaoui, S., Jelsch, C., Howard, J. A. K. & Lecomte, C. (1999). *Acta Cryst.* B**55**, 226–230.
Ellena, J., Goeta, A. E., Howard, J. A. K. & Punte, G. (2001). *J. Phys. Chem.* A**105**, 8696–8708.
Fabius, B., Cohen-addad, C., Larsen, F. K., Lehmann, M. S. & Becker, P. (1989). *J. Am. Chem. Soc.* **111**, 5728–5732.
Farrugia, L. J. (1997). *J. Appl. Cryst.* **30**, 565.
Frisch, M. J., Trucks, G. W., Sehlegel, H. B., Scuseria, G. E., Robb, M. A., Cheeseman, J. R., Zakrzewski, V. G., Montgomery, J. A. Jr, Stratmann, R. E., Burant, J. C., Dapprich, S., Millam, J. M., Daniels, A. D., Kudin, K. N., Strain, M. C., Farkas, O., Tomasi, J., Barone, V., Cossi, M., Cammi, R., Mennucci, B., Pomelli, C., Adamo, C., Clifford, S., Ochterski, J., Petersson, G. A., Ayala, P. Y., Cui, Q., Morokuma, K., Rega, N., Salvador, P., Dannenberg, J. J., Malick, D. K., Rabuck, A. D., Raghavaehari, K., Foresman, J. B., Cioslowski, J., Ortiz, J. V., Baboul, A. G., Stefanov, B. B., Liu, G., Liashenko, A., Piskorz, P., Komaromi, I., Gomperts, R., Martin, R. L., Fox, D. J., Keith, T., Al-Laham, M. A., Peng, C. Y., Nanayakkara, A., Challacombe, M., Gill, P. M. W., Johnson, B., Chen, W., Wong, M. W., Andres, J. L., Gonzalez, C., Head-Gordon, M., Replogle, E. S. & Pople, J. A. (2002). *GAUSSIAN*98. Revision A.11.3. Gaussian, Inc., Pittsburgh, PA, USA.
Hansen, N. K. & Coppens, P. (1978). *Acta Cryst.* A**34**, 909–921.
Hirshfeld, F. L. (1976). *Acta Cryst.* A**32**, 239–244.

Hooper, D. C., Wolfson, J. S., McHugh, G. L., Winters, M. B. & Swartz, M. N. (1982). *Antimicrob. Agents Chemother.* **22**, 662–671.
Howard, S. T., Hursthouse, M. B., Lehmann, C. W., Mallinson, P. R. & Frampton, C. S. (1992). *J. Chem. Phys.* **97**, 5616–5630.
Khalfan, H., Abuknesha, R., Rond-Weaver, M., Price, R. G. & Robinson, R. (1987). *Chem. Abstr.* **106**, 63932.
Koritsanszky, T., Howard, S., Su, Z., Mallinson, P. R., Richter, T. & Hansen, N. K. (1999). *XD. Computer Program Package for Multipole Refinement and Analysis of Electron Densities from Diffraction Data.* Free University of Berlin, Germany.
Maroncelli, M. & Fleming, G. R. (1987). *J. Chem. Phys.* **86**, 6221–6239.
Martin, A. & Pinkerton, A. A. (1998). *Acta Cryst.* B**54**, 471–477.
Morris, A. & Russell, A. D. (1971). *Prog. Med. Chem.* **8**, 39–59.
Munshi, P. & Guru Row, T. N. (2001). *Acta Cryst.* E**57**, o1175–o1176.
Munshi, P. & Guru Row, T. N. (2002). *Acta Cryst.* E**58**, o353–o354.
Scherer, W., Spiegler, M., Pedersen, B., Tafipolsky, M., Heiringer, W., Reinhard, B., Downs, A. J. & McGrady, S. (2000). *Chem. Commun.* pp. 635–636.
Sheldrick, G. M. (1997). *SHELXS*97. *SHELXL*97. University of Göttingen, Germany.
Slouf, M., Holy, A., Petricek, V. & Csarova, I. (2002). *Acta Cryst.* B**58**, 519–529.
Vishnumurthy, K., Guru Row, T. N. & Venkatesan, K. (2001). *Observations on the Photochemical Behavior of Coumarins and Related Systems in the Crystalline State. Understanding and Manipulating Excited-State Processes*, edited by V. Ramamurthy & K. S. Schanze, pp. 427–460. *Molecular and Supramolecular Photochemistry*, Vol. 8. New York/Basel: Marcel Dekker.
Volkov, A., Wu, G. & Coppens, P. (1999). *J. Synchrotron Rad.* **6**, 1007–1015.
Weber, H. P. & Craven, B. M. (1987). *Acta Cryst.* B**43**, 202–209.